

Received May 29, 2020, accepted June 24, 2020, date of publication July 3, 2020, date of current version July 16, 2020.

Digital Object Identifier 10.1109/ACCESS.2020.3006859

# Geolocation of Multiple Noncooperative Emitters Using Received Signal Strength: Sparsity, Resolution, and Detectability

KURT BRYAN<sup>1</sup>, (Member, IEEE), AND DEBORAH J. WALTER<sup>2</sup>, (Member, IEEE)

<sup>1</sup>Department of Mathematics, Rose-Hulman Institute of Technology, Terre Haute, IN 47803, USA

<sup>2</sup>Department of Electrical and Computer Engineering, Rose-Hulman Institute of Technology, Terre Haute, IN 47803, USA

Corresponding author: Kurt Bryan (kurt.bryan@rose-hulman.edu)

This work was supported in part by the Air Force Office of Scientific Research (AFOSR) under Grant FA9550-15-F-0001.


**ABSTRACT** In this paper we investigate the problem of locating multiple non-cooperative radio frequency (RF) emitters using only received signal strength (RSS) data. We assume that the number of emitters is unknown and that individual emitters cannot be distinguished in the RSS data. Moreover, we assume that the environment in which the data has been collected has not been mapped or “fingerprinted” by the prior collection of RSS data. Our goal is to use knowledge of the data noise level, sensor geometry, signal attenuation model, and other variables to quantify the limiting resolution that can be obtained with this type of data, and to determine the lowest power emitters that can be detected. We use this analysis to develop an efficient algorithm for estimating the number of emitters, their locations, and their transmit powers. We approach this by formulating the recovery problem as one of sparse approximation or compressed sensing. We illustrate the reasonableness of our assumptions and conclusions with both simulated and real data.

**INDEX TERMS** Source localization, compressed sensing, detection algorithms, signal mapping, sensor networks.

## I. INTRODUCTION

Locating radio frequency (RF) sources from remotely collected RF data is an important task in many settings, and is commonly referred to as RF *localization*, or *geolocation*. Applications are numerous, for example, the localization of subscribers in cell phone or other wireless networks (indoor or outdoor, see [1]–[5]). Localizing transmitters in a cognitive radio network ([6]–[8]) allows for the more efficient allocation of network resources, for example, frequency bands. Autonomous vehicles may rely on RF localization to augment navigation [6]. In military applications one may be tasked with geolocating RF transmitters that are non-cooperative or evasive [6], [9]–[12]. The detection and localization of drones flying in controlled or restricted airspace has become a pressing issue in the past few years ([13]–[16]). See [1] for a number of other applications.

A variety of techniques for localizing RF emitters from remote data have been developed. Some techniques use range

The associate editor coordinating the review of this manuscript and approving it for publication was Yongqiang Zhao .

information deduced from the signal time-of-arrival (TOA), time-difference-of-arrival (TDOA), or the received signal strength (RSS), perhaps collected from multiple sensors at spatially diverse locations. Others, such as angle-of-arrival (AOA), rely on directional information collected from sensors. One may or may not have information about the nature of the RF signals, e.g., emitted power or correlation of measured data from distinct sensors. The accuracy of the resulting position estimates depends on uncertainties in the channel models, sensor placement, and precision of the data collected.

The accuracy of RSS as a method for geolocation is known to suffer from large and small-scale propagation effects such as multipath and shadowing effects, but RSS-based localization methods have the advantage that sensor design can be low-complexity; complicated timing, synchronization, or other sophisticated hardware is not needed. Thus, the sensors can be relatively low-cost and low-power. The availability of such sensors is particularly important when many sensors are required, or the sensors are required to be battery-powered (e.g., remote or mobile sensors). Since received signal strength indicator (RSSI) values are available

directly from systems implementing standard communication protocols (see for example, [17]), many WLAN applications do not need any additional hardware to implement RSS-based localization algorithms.

In this work we examine the problem of geolocating multiple non-cooperative RF emitters using RSS measurements from multiple sensors dispersed geographically. Our focus is the case in which there are an unknown number of emitters and these emitters cannot be distinguished by frequency band or modulation scheme, or by decoding any signal information. In particular, we are interested in methods for estimating the number of emitters present, for quantifying the resolution one can obtain from RSS-based localization, and for determining the lowest power emitters that can be detected. These quantities depend on the number of sensors and their placement, the accuracy of the pathloss model, and the noise level in the data. We approach this analysis by formulating the recovery problem in the framework of compressed sensing or sparse approximation. We then use this analysis to inform and improve a recovery algorithm based on orthogonal matching pursuit (OMP). We emphasize that we assume the number of emitters is not known a priori and so must be ascertained from the data. Our methods are not tied to a specific scenario or geometry, but for illustrative purposes we focus on the setting of an outdoor environment in which a number of RF sensors on the ground (with known locations) are used to localize an unknown number of RF emitters mounted on drones, the situation considered in references [13]–[16].

Localization of RF sources from RSS data has been considered before ([2], [4], [18]–[20]) in a variety of scenarios. Some ([2], [21]–[23]) have taken the rough approach we use—a compressed sensing view that exploits spatial sparsity by assuming a small number of emitters are present. But many focus on situations in which the emitters are cooperative [18], or only one emitter is present, or emitters can be distinguished in some manner in the data ([19], [22], [24]). The interesting recent paper [25] considers the problem of multiple directional RF emitters, although the authors assume the number of emitters is known a priori, and they use an additive noise model rather than the more conventional log-normal noise model. They also provide a Cramer-Rao based estimate on the accuracy that their methods might attain. The paper [26] further develops Cramer-Rao bounds for emitter locations, powers, directions, and for pathloss exponents, under the assumption of a log-normal noise model. The authors also propose additional algorithms, but still work with a known number of emitters. They also appear to operate at a somewhat lower noise level than the scenarios presented in this paper.

Since RSS-based localization relies on a propagation model relating signal strength and distance to an emitter(s), RSS-based methods suffer if the signal strength model is inaccurate. Hence some prior work ([2], [18], [21], [27]) assumes that the environment has been “fingerprinted,” that is, sensors have been placed in known locations (“anchors”, [28]), and then empirical measurements

are taken to map the RF environment. This improves the channel model and accuracy of emitter location estimates. Some methods focus on prediction of lower bounds for the variance of location estimates from RSS data [29]–[31], and the above-mentioned [25], [26].

In our analysis we assume:

- The number of emitters is not known a priori, but must be determined from the data.
- Emitter signals cannot be distinguished by any characteristics in the time or frequency domain, and the RSS data collected by any sensor is the “aggregate” power summed over all emitters.
- The RF sensors are “limited” in number and have isotropic sensitivity, so no directional information is available.

From such data we seek to recover the number of emitters, the location of each, and the power at which each emitter transmits. In our analysis we employ the accepted log-normal noise model for RSS data with realistic noise levels.

## CONTRIBUTIONS

The unique contributions outlined in this paper are:

- A method to quantify the limiting resolution (ability to distinguish two close emitters) for this type of data, as a function of the data noise/uncertainty level, sensor placement, channel attenuation model, and other relevant physical parameters.
- A method to determine the limiting power threshold for an emitter’s “detectability” (the lowest power emitter than can be detected) as a function of the above-mentioned quantities, and the emitter’s location.
- The development of an appropriate algorithm that makes use of the above assumptions and can reliably estimate the actual number of emitters present, as well as their locations and powers.
- The use of this algorithm to illustrate our conclusions on resolution and emitter detectability, using both simulated and real data.

In Sections II and III below we formulate the problem of locating RF emitters from RSS data as one of finding a sparse solution to an underdetermined linear system of equations, and include an appropriate noise model. We then briefly review the notion of *coherence*, which plays an important role in our analysis of resolution and emitter detectability, and then briefly examine an appropriate algorithm for solving the resulting system. In Section IV we analyze the resolution that can be obtained with this type of data, and the power limits on emitter detectability. We then use this analysis to improve the algorithm and further illustrate our conclusions with computational examples. Finally, in Section V we detail actual data we collected to validate our model parameters, geolocate an emitter from measured RSS data, and provide additional illustrations of our conclusions.

## II. PROBLEM FORMULATION

### A. SYSTEM MODEL

Our analysis is not limited to any particular configuration of emitters and sensors, but as mentioned, we focus on a scenario in which one or more emitters are airborne, e.g., mounted on drones, and we wish to detect them using RSS data from a ground-based network of sensors. Specifically, let  $\Omega \subset \mathbb{R}^2$  and assume the emitters are at three-dimensional coordinates  $(x, y, h)$  with  $(x, y) \in \Omega$  and  $z = h \geq 0$ . Note that we are assuming the drones fly at a fixed, known altitude, but this assumption is not essential to the analysis below.

When the number of emitters is sufficiently small, localizing them is a problem well-suited to formulation in the context of compressed sensing, that of finding a sparse solution to a linear system of equations, where “sparse” means that most components in the relevant solution vector are zero (or close to zero). Specifically, let  $S = \cup_{i=1}^N \mathbf{r}_i$ , where  $\mathbf{r}_i = (x_i, y_i)$ , be a subset of  $N$  distinct points in  $\Omega$ ; the points  $(x_i, y_i, h)$  will be the potential locations of any emitters, where  $h \geq 0$  is the altitude at which the emitters operate. These points should be chosen to provide a reasonable sampling of the potential locations of any emitters. For example, if  $\Omega$  is a rectangle it may be convenient to define  $S$  as the nodes on a finely-spaced rectangular grid. It is not important that emitters be located precisely at any of these nodes.

Suppose there are  $M$  sensors that measure the RSS at known  $(x, y)$  positions  $\mathbf{s}_j = (a_j, b_j)$ , each at ground level (altitude 0) in the  $xy$ -plane. We take each at the same altitude only for simplicity; the sensors need not be at a single altitude nor in  $\Omega$ . We assume that the sensors’ antennas are isotropic, though more realistic antenna patterns are easily accommodated in the analysis. The distance  $r_{ij}$  from the  $j$ th sensor to the  $i$ th potential emitter location is  $r_{ij} = \sqrt{\|\mathbf{s}_j - \mathbf{r}_i\|_2^2 + h^2}$  where  $\|\cdot\|_2$  denotes the usual Euclidean norm in the plane.

One common model for the power  $P_{ij}$  received at sensor  $j$  from an emitter at position  $\mathbf{r}_i$  is that  $P_{ij} = p_i(r_0/r_{ij})^n$  where  $p_i \geq 0$  is a reference power measured at distance  $r_0$  from the emitter  $i$  and  $n$  is the *pathloss exponent* that governs the attenuation of the signal power as a function of distance; see [10], [34]. In the ideal case the RSS at sensor  $j$  from all emitters is then modeled as

$$d_j = \sum_{i=1}^N P_{ij} = \sum_{i=1}^N p_i \left( \frac{r_0}{r_{ij}} \right)^n. \quad (1)$$

This assumes receiver antennas are equally sensitive, isotropic, and that the emitters are isotropic and incoherent. If no emitter is present at position  $\mathbf{r}_i$  then  $p_i = 0$ , so if few emitters are present then we expect  $p_i > 0$  for only a few indices  $i$ .

We amalgamate the data  $d_j$  into a column vector  $\mathbf{d}_0 \in \mathbb{R}^M$  and express the ideal RSS data (1) in matrix form,

$$\mathbf{d}_0 = \Phi \mathbf{p}_0. \quad (2)$$

Here  $\Phi$  is the *measurement matrix*, an  $M \times N$  matrix with known entry  $(r_0/r_{ij})^n$  in row  $i$ , column  $j$ . The vector  $\mathbf{p}_0 \in \mathbb{R}^N$

has  $i$ th entry  $p_i$ , the reference power of the emitter at  $\mathbf{r}_i$ , and is sparse if few emitters are present. Note that the entries of  $\Phi$  are known. The  $j$ th row of  $\Phi$  embodies the data from the sensor at position  $\mathbf{s}_j$ , and the  $i$ th column corresponds to a potential emitter location  $\mathbf{r}_i$ . We assume that we can measure the quantity  $\mathbf{d}_0$ , the power received by each sensor. The problem of interest is to recover an estimate of  $\mathbf{p}_0$  from  $\mathbf{d}_0$  and  $\Phi$ . Of course  $\mathbf{d}_0$  will be corrupted by noise or other error.

### B. MEASUREMENT NOISE MODEL

Departure of measured RSS data from the ideal model above is considered at length in, for example, [35]. We assume that data has been suitably processed to eliminate the effects of so-called “fast-fading” as recommended in [35] and that after this processing the error that remains conforms to the standard log-normal noise model. Specifically, if an emitter with reference power  $p_i$  is present at location  $\mathbf{r}_i$ , the contribution to the data  $d_j$  collected at the  $j$ th sensor from this emitter is of the form

$$d_j = p_i \left( \frac{r_0}{r_{ij}} \right)^n e^{\eta R_i}$$

where  $\eta = \ln(10)/10$  and  $R_i$  is a normal random variable with mean 0 and standard deviation  $\sigma_{dB}$ . Note that  $e^{\eta R_i} = 10^{R_i/10}$ . Here  $\sigma_{dB}$  is the noise level in dB. Values for  $\sigma_{dB}$  vary widely depending on the setting, but for the application of interest here (outdoors, a relatively open and obstruction-free area) values from 2 to 5 dB or higher are common; see [18] or our data in Section V-A.

For multiple emitters we take

$$d_j = \sum_{i=1}^N p_i \left( \frac{r_0}{r_{ij}} \right)^n e^{\eta R_{ij}} \quad (3)$$

with the additional assumption that the  $R_{ij}$  are independent.

### C. UNDERDETERMINED SYSTEMS, COHERENCE, AND SPARSE SOLUTIONS

Let  $\mathbf{d} \in \mathbb{R}^M$  denote the noisy data vector with components given by (3). Under the assumption that the number of sensors is much smaller than the number of potential emitter locations ( $M \ll N$ ), the system  $\Phi \mathbf{p} = \mathbf{d}$  to be solved for  $\mathbf{p}$  (an estimate of  $\mathbf{p}_0$ ) is underdetermined, and so almost certainly possesses infinitely many solutions. However, as noted we will make the reasonable assumption that there are few emitters, so that the solution vector  $\mathbf{p}_0$  is sparse. More specifically, a vector  $\mathbf{p}$  is said to be *k-sparse* if  $\mathbf{p}$  has at most  $k$  nonzero components. Under the assumption that  $\mathbf{p}_0$  is *k-sparse* for sufficiently small  $k$ , it is highly likely that a physically relevant solution can be found, although the existence of a unique sparse solution and the ease with which it can be found depend on the measurement matrix  $\Phi$ .

One property that  $\Phi$  can possess that leads to favorable recovery results is that of low “mutual coherence.” First,

the *coherence* of vectors  $\mathbf{x}, \mathbf{y} \in \mathbb{R}^N$  is the quantity

$$\mu(\mathbf{x}, \mathbf{y}) = \frac{|\mathbf{x} \cdot \mathbf{y}|}{\|\mathbf{x}\|_2 \|\mathbf{y}\|_2}. \quad (4)$$

The Cauchy-Schwarz inequality shows that  $0 \leq \mu(\mathbf{x}, \mathbf{y}) \leq 1$ , with  $\mu(\mathbf{x}, \mathbf{y}) = 0$  when  $\mathbf{x}$  and  $\mathbf{y}$  are orthogonal and  $\mu(\mathbf{x}, \mathbf{y}) = 1$  when one vector is a scalar multiple of another. The *mutual coherence* of an  $M \times N$  matrix  $\Phi$  with columns  $\Phi_i$  is the quantity

$$\mu(\Phi) = \max_{i \neq j} \mu(\Phi_i, \Phi_j). \quad (5)$$

Again,  $0 \leq \mu(\Phi) \leq 1$ . If  $\mu(\Phi) = 1$  then two or more distinct columns of  $\Phi$  are scalar multiples of each other, while  $\mu(\Phi) = 0$  means  $\Phi$  is an orthogonal matrix, which is impossible in the present situation since  $M < N$ .

Low coherence matrices are desirable when seeking sparse solutions to a linear system  $\Phi \mathbf{p} = \mathbf{d}$ . It can be shown that if  $\mu(\Phi) < 1/(2k-1)$  then any  $k$ -sparse solution  $\mathbf{p}$  is unique and many compressed sensing algorithms will converge to this solution (see Section 5.1 of [36]). Low mutual coherence also leads to more favorable bounds on the error in the presence of noisy data [37].

Unfortunately, for the localization problem described above, low mutual coherence will not hold for any realistic sensor configuration. First, our measurement matrix has entirely positive entries, so no cancelation occurs in the dot product of columns of  $\Phi$ ; as a result, the pairwise coherence for any two columns is likely to be larger than for a matrix with mixed sign entries. Also, if potential emitter locations  $(x_i, y_i)$  and  $(x_j, y_j)$  are closely spaced, then the  $i$ th and  $j$ th columns  $\Phi_i$  and  $\Phi_j$  of the measurement matrix will be nearly identical, and so have high pairwise coherence. Thus, if we work on a fine grid (to obtain higher source resolution) we confront measurement matrices with high mutual coherence. This presents a challenge for the finding the correct sparse solution.

### III. ALGORITHM FOR SPARSE SOLUTIONS

In this section we briefly detail an algorithm appropriate for finding sparse solutions to the problem at hand. We then use this algorithm to gain insight into the ill-posedness of this inverse problem, and provide examples that illustrate the analysis for resolution and clearance. In Section IV-E we use our analysis to propose an improvement to this algorithm, which we illustrate with simulated and real data.

#### A. BLOOMP

Finding the sparsest solution to a linear system of equations is, in general, computationally intractable, even if a sparse solution is known to exist [38]. However, a number of efficient computational approaches have been devised that, under the right conditions, find such a sparse solution with high probability. In this section we justify use the algorithm “Band-excluded Locally Optimized Orthogonal Matching Pursuit” (BLOOMP, see [39]) for the present problem, and include an illustrative computational example.

Briefly, the BLOOMP algorithm is a modification of Orthogonal Matching Pursuit (OMP). OMP is a “greedy” algorithm that iteratively builds up a sparse solution to  $\Phi \mathbf{p} = \mathbf{d}$  one nonzero component at a time. Let  $\mathbf{p}^0 = \mathbf{0}$  denote our initial guess at a solution,  $\mathbf{p}^k$  the  $k$ th iterate (at most  $k$ -sparse) in OMP, and  $S^k = \{i : \mathbf{p}_i^k \neq 0\}$ ;  $S^k$  is called the *support* set of  $\mathbf{p}^k$ . The set  $S^k$  indexes those columns of  $\Phi$  that are being used to synthesize the data  $\mathbf{d}$ . OMP constructs  $\mathbf{p}^{k+1}$  by augmenting the support  $S^k$  with a new index  $i_k$  chosen so that the residual  $\|\Phi \mathbf{p}^{k+1} - \mathbf{d}\|_2$  is minimized. This continues until a maximum sparsity bound or a termination criterion is met. One common stopping criterion takes the form  $\|\Phi \mathbf{p}^k - \mathbf{d}\|_2 \leq C\epsilon$  where  $\epsilon$  is comparable to the expected noise level in the data as measured in the Euclidean norm and  $C \approx 1$ ; see [36]. We say more on this in our specific application below in Section III-B and Appendix VI.

A drawback of OMP is that once an index has been added to the support set  $S^k$ , it is never removed at a later iteration, so sub-optimal early choices cannot be undone. Many modifications to OMP have been proposed to overcome this problem. We have adopted one such modification, BLOOMP [39], because it is particularly suited to “high-coherence” measurement matrices. Like OMP, BLOOMP builds a sparse solution by adding one index at each iteration to the potential support set. In our application this means adding one estimated emitter at each iteration. However, in the BLOOMP algorithm the column in  $\Phi$  corresponding to the emitter added at a given iteration cannot have high coherence with any column of  $\Phi$  corresponding to previously added emitters. Physically, the next estimated emitter location cannot be too close to those already determined to be present—this is the “band exclusion” modification of OMP. Moreover, at each iteration the emitters currently estimated to be present are subject to local adjustments in location and power to better fit the data; this is the “local” optimization portion of the algorithm.

The authors in [39] show that in situations such as these—high coherence matrices, but in which the correct solution index support corresponds to columns with lower pairwise coherence, such as well-separated emitters on a finely-spaced grid—the BLOOMP modifications to OMP increase the probability of recovering the correct solution support indices, or in the setting of this paper, the correct emitter number and location(s). In our setting this strategy gives a substantial improvement in the recoveries, compared to OMP. We also add a constraint to the algorithm to require that at each iteration the emitter power estimates must remain nonnegative, which further stabilizes recoveries.

#### EFFICIENCY AND TIMING

Standard OMP for an  $M \times N$  measurement matrix has a complexity of about  $O(sMN)$  operations, where  $s$  is the sparsity of the solution recovered by OMP (also the number of iterations taken by OMP) [40]. In our setting  $s$  would be comparable to the maximum number of emitters we expect to be present. The additional steps taken to modify OMP into BLOOMP do



not affect this asymptotic complexity. The execution times for the BLOOMP algorithm on this problem are quite small. In the computational experiments detailed in the next section reconstructions were performed in Matlab running on an i7 laptop. In this setting, when seeking  $s = 3$  emitters using  $M = 30$  sensors and  $N = 2500$  potential emitter locations, a complete reconstruction takes approximately 0.4 seconds.

**B. RECOVERY EXAMPLE**

To illustrate, let  $\Omega$  be the  $50 \times 50$  meter region  $\{(x, y); 0 \leq x, y \leq 50\}$  and consider a  $50 \times 50$  rectangular grid for potential emitter locations, of the form  $(x_i, y_j)$  where  $x_i = (i - 0.5), y_j = (j - 0.5)$  for  $1 \leq i, j \leq 50$ , so here  $N = 50^2 = 2500$ . In many settings it is the case that randomness in the construction of the measurement matrix is an asset in using sparsity or compressed sensing recovery algorithms [41]. We thus consider  $M = 30$  RSS data points collected from 30 RSS sensors on the ground in  $\Omega$ . The sensor locations are displayed as crosses in Fig. 1. We use pathloss exponent  $n = 3.5$  in equation (1) (assumed known for now) and noise level  $\sigma_{dB} = 3$  dB in equation (3); this corresponds to a signal-to-noise ratio of about 1 : 1 in the log-normal noise model. See Section V for data that supports these parameter choices, and for a recovery from measured data.

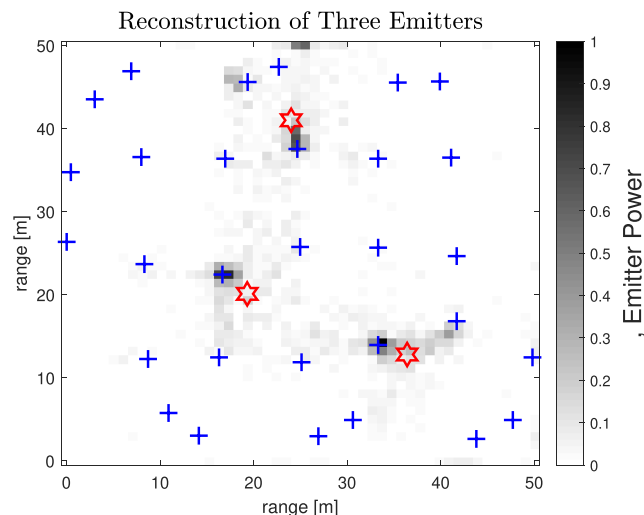


**FIGURE 1.** Average recovered power from 500 simulation runs (white is 0 power, black is power 1 or higher). The true emitters are marked as stars, sensor locations as crosses. The log-normal randomized noise is simulated with  $\sigma_{dB} = 3$ .

Three emitters with unit power at reference distance  $r_0 = 1$  meter are present at  $(x, y)$  positions (24.0, 41.0), (19.3, 20.1), and (36.4, 12.8), at a known altitude of 10 meters (hereafter referred to as emitters 1, 2, and 3, respectively); these could correspond to emitters associated with drones in the area. Note that these  $(x, y)$  coordinates are not themselves grid points, nonetheless one would hope to recover emitter estimates that correspond to nearby grid points. We then simulate noisy data  $\mathbf{d}$  using equation (3) and perform a reconstruction from  $\mathbf{d}$  using the BLOOMP algorithm, to recover an estimate

of the emitter number, location(s), and power(s). This process of generating noise and reconstructing is repeated 500 times, each with a different noise realization. We emphasize that the number of emitters is not assumed a priori.

One can show (see Appendix VI) that for a modest noise level  $\sigma_{dB} \leq 5$  dB the expected value of  $\|\mathbf{d} - \mathbf{d}_0\|_2^2$  is bounded by and comparable to the quantity  $\epsilon = (\mu_0^2 + \sigma_0^2)\|\mathbf{d}_0\|_2^2$  where  $\mu_0 = e^{\eta^2 \sigma_{dB}^2 / 2} - 1$  and  $\sigma_0^2 = e^{\eta^2 \sigma_{dB}^2} (e^{\eta^2 \sigma_{dB}^2} - 1)$  (recall  $\eta = \ln(10)/10$ ). Of course the noiseless data  $\mathbf{d}_0$  is unknown, but the noisy data  $\mathbf{d}$  provides a reasonable estimate. We thus terminate the iteration when the fit to the data is comparable to (or a bit smaller than) this noise level, specifically, when

$$\|\mathbf{d} - \mathbf{d}_k\|_2 \leq C \sqrt{(\mu_0^2 + \sigma_0^2)} \|\mathbf{d}\|_2 \tag{6}$$

where  $\mathbf{d}_k = \Phi \mathbf{p}^k$  denotes the estimated data at the  $k$ th iteration of BLOOMP and  $C$  is a constant less than or equal to 1 (we use  $C = 1/4$ ). For high noise levels the random variable  $\|\mathbf{d} - \mathbf{d}_k\|_2$  is more highly skewed to the right, and so  $E(\|\mathbf{d} - \mathbf{d}_k\|_2)$  may be somewhat smaller than  $\sqrt{\|\mathbf{d} - \mathbf{d}_k\|_2^2}$ . In this case a value of  $C$  somewhat less than 1 can be helpful to prevent the iterative algorithm from terminating too early.

As mentioned above, all simulations were performed in Matlab running on an i7 laptop computer, with each individual reconstruction of emitter locations requiring about 0.4 seconds. A typical reconstruction does 4 to 6 iterations of the BLOOMP algorithm. The results of these 500 simulated cases are shown in Fig. 1. The image is an average of the recovered power at each grid location, coded so 0 recovered power is white, 1 or higher is black. The sensor locations are illustrated as crosses and the true position of each emitter is represented by a star. The average estimated power for each of the three emitters is 1.7424, 0.8830, and 1.1712 for emitters 1, 2, and 3. The gray areas indicating positive power recovery clustered around the three emitters, which are reasonably well resolved. An analysis of this resolution is the focus of the next section.

It should also be emphasized that Fig. 1 is an average of 500 reconstructions; any individual reconstruction yields only a few estimated emitters. In this case the average number of emitters per reconstruction was 5.17. In Section IV-E we propose a strategy for “cleaning up” any given reconstruction by eliminating emitters that are likely spurious estimates.

One might expect that the pathloss exponent  $n$  to be a rather critical value in estimating the number and position of the emitters, but we find that this is not the case. Specifically, an incorrect pathloss exponent has little effect on the recovery of the emitter count and locations, but does significantly affect the estimated power of each emitter. As an illustration, in Fig. 2 is shown a recovery with exactly the same parameters as Fig. 1, but with the (erroneous) assumption of a pathloss exponent of 2.5 (whereas  $n = 3.5$  was used to simulate the data). The average estimated power is 0.1368, 0.0595, and 0.0612 for emitters 1, 2, and 3, respectively; this is considerably off from the correct values of 1 for each. Nonetheless, the number and location are quite accurate.

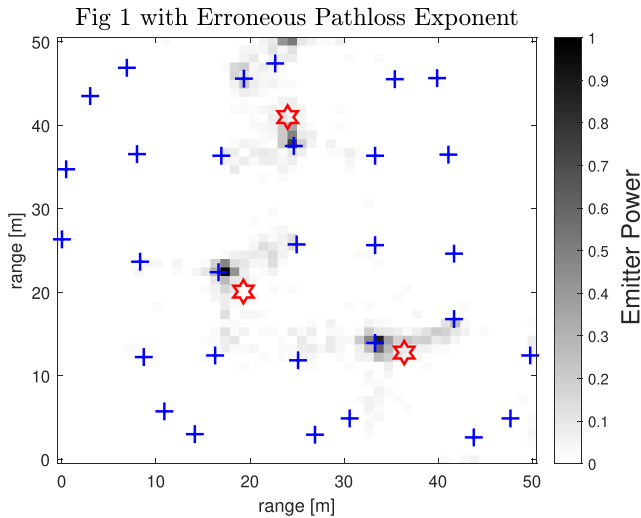


**FIGURE 2.** Average recovered power from 500 simulation runs (white is 0 power, black is power 1 or higher), erroneous pathloss exponent. The true emitters are marked as stars, sensor locations as crosses. The log-normal randomized noise is simulated with  $\sigma_{dB} = 3$ .

**IV. ANALYSIS OF RESOLUTION AND DETECTION LIMITS**

The goal in this section is to develop a method for quantifying the local resolution one can obtain at any fixed potential emitter location from RSS data for a given noise level and sensor configuration, and to provide a bound on the weakest emitters that can be reliably detected. We then consider how this analysis can be used to improve the location algorithm.

**A. RESOLUTION ANALYSIS**

Suppose an emitter lies on one of two potential locations, say  $\mathbf{q}_1 = (x_1, y_1)$  or  $\mathbf{q}_2 = (x_2, y_2)$ . We collect noisy RSS data from  $M$  sensors. The goal is to determine at which location the emitter actually lies, with sufficiently high probability (to be specified). If this can be done we will say the two potential locations are “resolvable.”

Let  $\mathbf{d}_k \in \mathbb{R}^M$  denote the noiseless RSS data we would collect from an emitter at location  $\mathbf{q}_k$ , where  $k = 1$  or  $k = 2$ . This data vector is assumed to obey the model (1), with a single nonzero power location. For convenience we define normalized data vectors

$$\mathbf{b}_1 = \frac{\mathbf{d}_1}{\|\mathbf{d}_1\|_2} \text{ and } \mathbf{b}_2 = \frac{\mathbf{d}_2}{\|\mathbf{d}_2\|_2} \tag{7}$$

so  $\|\mathbf{b}_k\|_2 = 1$  for  $k = 1, 2$ . Note that the reference power  $p_k$  will not matter in either case.

Suppose we collect noisy data  $\mathbf{d} \in \mathbb{R}^M$  from the sensors, stemming from an emitter at location  $\mathbf{q}_1$ ; the components of  $\mathbf{d}$  are given by (3) (with only a single nonzero summand). The goal is to use  $\mathbf{d}$  to correctly assign the emitter to location  $\mathbf{q}_1$ , as opposed to  $\mathbf{q}_2$ . If we formulate this as a compressed sensing problem as above in equation (2) then we obtain linear system

$$\begin{bmatrix} \mathbf{b}_1 & \mathbf{b}_2 \end{bmatrix} \begin{bmatrix} p_1 \\ p_2 \end{bmatrix} = \mathbf{d}$$

(equivalently,  $p_1\mathbf{b}_1 + p_2\mathbf{b}_2 = \mathbf{d}$ ) in which the sensing matrix  $\Phi$  is  $M \times 2$  with unit norm columns  $\mathbf{b}_1$  and  $\mathbf{b}_2$ . We seek a 1-sparse solution to this system. In this very simple case OMP or any standard sparse solver (e.g., basis pursuit) will provide a 1-sparse solution consisting of a multiple of that column of  $\Phi$  which has the highest coherence with the data  $\mathbf{d}$ , with power estimate  $\tilde{p}_k = \mathbf{b}_k \cdot \mathbf{d}$  for either  $k = 1$  or  $k = 2$ . That is, the emitter is correctly assigned to location  $\mathbf{b}_1$  if

$$\mu(\mathbf{b}_1, \mathbf{d}) > \mu(\mathbf{b}_2, \mathbf{d}) \tag{8}$$

and incorrectly to location  $\mathbf{p}_2$  otherwise. Condition (8) is quite natural—the emitter is assigned to a location according to which vector  $\mathbf{b}_1$  or  $\mathbf{b}_2$  best matches the collected data  $\mathbf{d}$  after normalizing for power. This notion of resolution is not wedded to a compressed sensing approach to the problem, nor any particular algorithm.

Equation (8) is equivalent to

$$\mathbf{c} \cdot \mathbf{d} > 0 \tag{9}$$

where

$$\mathbf{c} = \mathbf{b}_1 - \mathbf{b}_2. \tag{10}$$

Equations (9) and (10) can be written equivalently as  $Q > 0$  where

$$Q = \sum_{j=1}^M w_j e^{\eta R_j} \tag{11}$$

with  $w_j = c_j/r_{1j}^n$  and where  $c_j$  denotes the  $j$ th component of  $\mathbf{c}$ . For a given sensor configuration the  $w_j$  are known. We want to compute the probability  $P(Q > 0)$ , so that we correctly assign the emitter to location  $\mathbf{q}_1$ . It should be noted that we will have  $0.5 \leq P(Q > 0) \leq 1$ , with  $P(Q > 0) = 1$  as the best case—the emitters are certainly resolvable—and  $P(Q > 0) = 0.5$  as the worst case, in which resolving the emitter locations becomes a “coin toss.”

The random variable  $Q$  is a signed linear combination of log-normal random variables (the  $w_i$  are generally of mixed sign). The next section is devoted to accurately approximating the probability  $P(Q > 0)$  in an easily computable fashion.

**B. APPROXIMATING A SIGNED SUM OF LOG-NORMAL RANDOM VARIABLES**

Though  $Q$  has coefficients of mixed sign, we first consider the case in which all coefficients are positive. The distribution of such a sum of log-normals is a well-studied problem, though such a sum has no closed-form density function. However, it has long been noted that such a sum is itself approximately log-normal, and so can be characterized as being of the form  $e^{N(\mu, \sigma^2)}$  for suitable  $\mu$  and  $\sigma$ . Note that  $\mu$  stands for the mean of the noise distribution here, not mutual coherence.

In [42] the authors provide a simple and effective method for fitting  $\mu$  and  $\sigma$  to such a sum. The individual log-normals in the sums they consider are of the form  $e^{N(\mu_j, \sigma_j^2)}$  with varying  $\mu_j$  and  $\sigma_j$ , and are assumed independent. For a linear

combination of the form (11) with weights  $w_j$  that are positive, the weighted sum in  $Q$  is easily adapted to this setting, by absorbing the  $w_j$  into the  $R_j$  (we can shift the mean of  $R_j$  by  $\ln(w_j)$ ). If we split the sum defining  $Q$  into a piece with positive weights and a piece with negative weights, we can write  $Q = Q^+ - Q^-$  where

$$Q^+ = \sum_{w_j \geq 0} w_j e^{\eta R_j} \text{ and } Q^- = \sum_{w_j < 0} (-w_j) e^{\eta R_j}. \quad (12)$$

The method of [42] provides a log-normal random variable approximation for  $Q^+$  in the form  $e^R$  where  $R = N(\mu_+, \sigma_+)$ , by determining an appropriate mean and variance  $\mu_+$  and  $\sigma_+^2$ . A similar approximation is made to obtain  $\mu_-$  and  $\sigma_-$  for  $Q^-$ .

The probability density function (pdf) and cumulative density function (cdf) for the log-normal random variable are well-known. Moreover, if a random variable  $X$  has cdf  $F(x)$  and random variable  $Y$  has pdf  $g(x)$  then the cdf  $H(x)$  for  $X - Y$  is given by

$$H(x) = \int_{-\infty}^{\infty} F(x + y)g(y) dy.$$

Then, for example,  $P(X - Y > 0)$  is given by  $1 - H(0)$ . In the present case the cdf  $H$  for  $Q = Q^+ - Q^-$  can be expressed as

$$H(x) = \int_{\max(0, -x)}^{\infty} \left[ \frac{1}{2} + \frac{1}{2} \operatorname{erf} \left( \frac{\ln(x + y) - \mu_+}{\sigma_+ \sqrt{2}} \right) \right] \times \left[ \frac{1}{y \sigma_- \sqrt{2\pi}} e^{-\frac{(\ln(y) - \mu_-)^2}{2\sigma_-^2}} \right] dy. \quad (13)$$

The  $\max(0, -x)$  lower limit in the integral in (13) cuts off the integral as soon as the cdf or pdf of either random variable equals zero. The value we are interested in is  $P(Q > 0) = 1 - H(0)$ , and this can be computed easily from (13).

The overall procedure is as follows: Given potential emitter locations  $\mathbf{q}_1$  and  $\mathbf{q}_2$ , we compute  $\mathbf{c}$  as in (10) and set  $w_j = c_j / r_{1j}^n$  with  $r_{1j}$  as the distance from location  $\mathbf{q}_1$  to the  $j$ th sensor. We then use the procedure in [42] to estimate  $\mu_+, \sigma_+, \mu_-$ , and  $\sigma_-$  for  $Q^+$  and  $Q^-$  and compute  $P(Q > 0)$  using (13). If  $P(Q > 0)$  exceeds some threshold probability  $p_{min}$  we will say the emitter location  $\mathbf{q}_1$  is resolvable from location  $\mathbf{q}_2$ .

To illustrate the accuracy of the approximation based on (13), Fig. 3 shows the quantity  $P(Q > 0) = 1 - H(0)$  computed by this procedure versus the simulated probability of correctly resolving the emitter locations for a variety of sensor counts and noise levels. In each base we use  $\mathbf{q}_1 = (24.5, 41.5)$  and  $\mathbf{q}_2 = (19.5, 20.5)$ , altitude  $h = 10$ , with sensors at random  $(x, y)$  locations in  $0 < x, y < 50$ . We generate  $10^4$  realizations of synthetic noisy data  $\mathbf{d}$  for a sensor at location  $\mathbf{q}_1$  and assign it to location  $\mathbf{q}_1$  if  $\mu(\mathbf{d}, \mathbf{b}_1) > \mu(\mathbf{d}, \mathbf{b}_2)$ , location  $\mathbf{q}_2$  otherwise. The pathloss exponent is 3.5.

To illustrate how this can be used to quantify local resolution, consider the three-emitter configuration of Fig. 1, with the same noise level and other parameters. What local resolution might we expect near the emitter at location  $(24, 41)$ ? Let  $\mathbf{p}_1 = (24, 41)$  and  $\mathbf{p}_2 = (x, y)$  for  $0 < x, y < 50$ ,

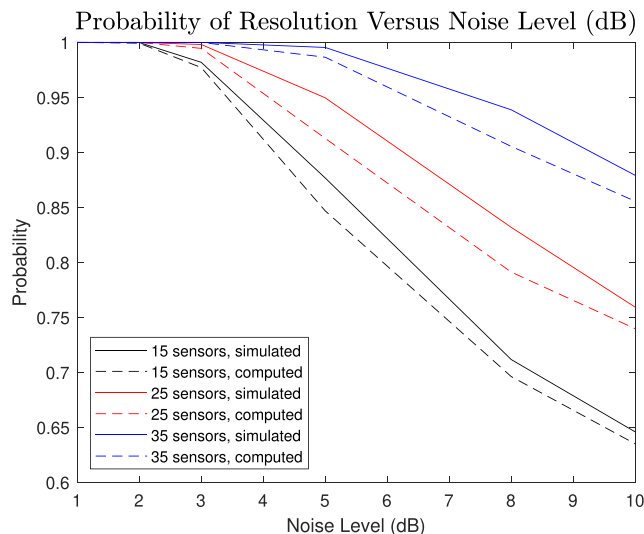


FIGURE 3. Simulated and approximated resolution probability for various sensor counts and noise levels.

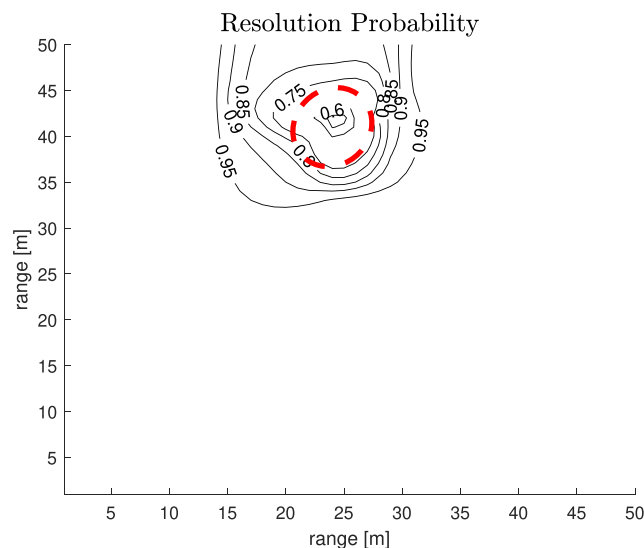
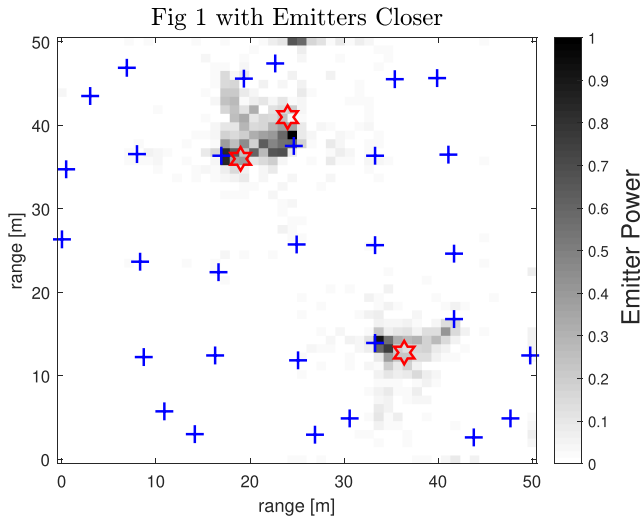


FIGURE 4. Probability of successful resolution as function of  $(x, y)$ . Red oval is a 95 percent confidence region from the Cramer-Rao bounds.

so that  $P(Q > 0)$  as computed above is a function of  $(x, y)$ . In Fig. 4 we show a contour plot of this function. The red oval delineates, for comparison, the Cramer-Rao lower bounds on the uncertainty in estimating the location of the emitter (further discussed in Subsection IV-C below).

To illustrate the validity of the resolution analysis, in Fig. 5 is shown a situation similar to that of Fig. 1, but in which the emitter at position  $(19.3, 20.1)$  has been moved to  $(19.0, 36.0)$ , which is only 7 meters away from the emitter at position at  $(24, 41)$ . The newly moved emitter lies outside the Cramer-Rao bounds, on about the  $P(Q > 0) = 0.85$  contour. The emitters are not as reliably resolved.

This analysis makes it clear that, for a given noise level (and other parameters) the resolution obtainable with RSS data is limited, and can be quantified. In particular, in a



**FIGURE 5.** Average recovered power from 500 simulation runs (white is 0 power, black is power 1 or higher). The true emitters are marked as stars, sensor locations as crosses.

compressed sensing approach there are little improvements in resolution to be obtained by using too fine of a grid.

**C. COMPARISON TO CRAMER-RAO BOUNDS**

Other authors (e.g., [29]–[31]) have examined statistical bounds, for example, Cramer-Rao bounds, on the minimum variance that can be obtained by using RSS data to estimate the distance to or position of an emitter. Such a bound provides a natural way to quantify resolution. However, as noted in [30] and [31], the Cramer-Rao bounds in this setting cannot be attained by any unbiased estimator, and so are too optimistic, especially at higher noise levels. It should also be noted that our estimates are almost certainly biased.

To illustrate and compare with the current analysis, we consider a single emitter of unknown power  $p_0$  at true location (22, 41), altitude zero, with the 30 sensor locations as used in Figs. 1, 4, and 2, pathloss exponent 3.5, and noise level 3 dB. Following the computations of Section 3.2 in [31] we establish a Cramer-Rao lower bound on the minimum covariance of any unbiased estimator of the emitter location and power. The red elliptical region in Fig. 4 is a 95 percent confidence region with respect to the spatial variables for an emitter with  $p_0 = 1$ , though the bounds do not depend on the unknown power  $p_0$ . These limits are considerably smaller than those given by our procedure, which more accurately reflect what to expect.

**D. DETECTABILITY AND CLEARANCE**

In this section we consider the problem of when we can be reasonably certain that we have detected all the emitters above a given power threshold in a region of interest; this could be the entire region  $\Omega$  or some subregion thereof. The bounds so established can be used to determine when a recovered emitter is spurious, and likely due solely to noise. Such a bound can also be used to inform a termination criterion in the search for emitters.

For a given configuration of  $M$  sensors,  $N$  potential emitter locations and corresponding  $M \times N$  measurement matrix  $\Phi$ , suppose that  $\mathbf{p}_0 \in \mathbb{R}^N$  embodies the true emitter power vector. The noise-free data  $\mathbf{d}_0 \in \mathbb{R}^M$  is given by (2); let  $\mathbf{d} \in \mathbb{R}^M$  be the collected (noisy) data vector. Suppose that  $\mathbf{p}_r$  is an estimate of  $\mathbf{p}_0$  based on the data  $\mathbf{d}$ , computed using BLOOMP or any other recovery algorithm. We assume, however, that the algorithm produces an estimate  $\mathbf{p}_r$  for which an error bound of the form  $\|\Phi\mathbf{p}_r - \mathbf{d}\| \leq \epsilon$  holds, for some tolerance  $\epsilon$ , where  $\|\cdot\|$  can denote any norm, e.g., the  $L^2$  or supremum norm. Typically  $\epsilon$  is comparable to the expected noise level in the data in the appropriate norm.

Now suppose that a single additional emitter were present at location  $\mathbf{r}_i$ , with power  $P$ . Let  $\tilde{\mathbf{p}} = \mathbf{p}_r + P\mathbf{e}_i$  denote resulting power vector ( $\mathbf{e}_i$  is the  $i$ th standard basis vector in  $\mathbb{R}^N$ ). This would yield data  $\tilde{\mathbf{d}} = \Phi\tilde{\mathbf{p}} = \Phi\mathbf{p}_r + P\Phi_i$ . We will consider the additional emitter at  $\mathbf{r}_i$  to be detectable if

$$\|\tilde{\mathbf{d}} - \mathbf{d}\| > \epsilon. \tag{14}$$

That is, the presence of this additional emitter would yield reconstructed data  $\tilde{\mathbf{d}}$  that is inconsistent with the measured data at the given tolerance level. But we do not require that the reconstructed emitter power configuration  $\mathbf{p}_r$  be accurate, in that  $\|\mathbf{p}_r - \mathbf{p}_0\|$  need not be small.

The value of  $P$  that assures  $\|\tilde{\mathbf{d}} - \mathbf{d}\| > \epsilon$  holds can be estimated. We have, using the reverse triangle inequality,

$$\begin{aligned} \|\tilde{\mathbf{d}} - \mathbf{d}\| &= \|P\Phi_i + \Phi\mathbf{p}_r - \mathbf{d}\| \\ &\geq |P\|\Phi_i\| - \|\Phi\mathbf{p}_r - \mathbf{d}\|| \\ &\geq P\|\Phi_i\| - \epsilon. \end{aligned}$$

Inequality (14) must hold if  $P\|\Phi_i\| - \epsilon > \epsilon$  or

$$P > \frac{2\epsilon}{\|\Phi_i\|}. \tag{15}$$

The threshold on the right in (15) depends on the precision to which we fit the measured data, i.e., the noise level in the data, the norm we use, and on  $\Phi$ . By taking the maximum of the right side of (15) over all locations  $\mathbf{r}_i$  in a given region  $\Omega' \subseteq \Omega$  we obtain a threshold of the weakest emitters that can be reliably identified in  $\Omega'$ . If a lower threshold is desired, it would be necessary to alter the number and/or placement of sensors. Inequality (15) quantifies what is required. Of course the estimates leading to (15) are likely pessimistic—an emitter may well be detected below this power threshold—but it does provide a rough lower bound for emitter detectability.

To illustrate, again consider the setting of Fig. 1. Let us consider the power threshold for detectability of the emitter at location (19.3, 20.1). The closest grid location is  $\mathbf{r}_{1020} = (19.5, 20.5)$  (that is, index location  $i = 1020$  in our indexing scheme). We iterate BLOOMP until  $\|\tilde{\mathbf{d}} - \mathbf{d}\|_2 \leq 2 \times 10^{-4}$  and compute  $\|\Phi_{1020}\|_2 \approx 3.56 \times 10^{-4}$ , leading to a power bound  $P \approx 1.1$  for the emitter in this location. As is obvious in Fig. 1, the emitter is clearly detectable at power level 1. However, under the same conditions but with power level 0.5 the result is as shown in Fig. 6. At power level 0.25 the emitter becomes essentially invisible.



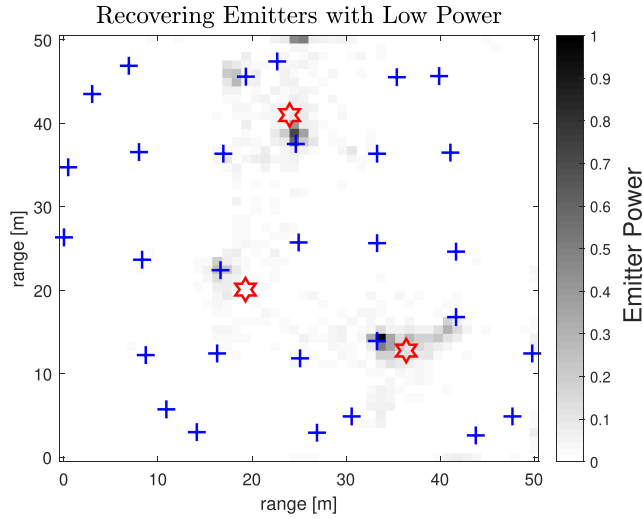


FIGURE 6. Setting of Fig. 1, but with emitter at (19.3, 20.1) at power 0.5.

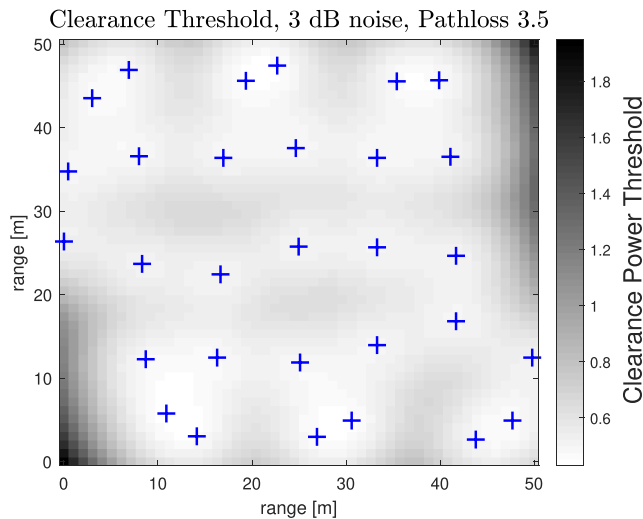


FIGURE 7. Clearance power threshold as function of position, setting of Fig. 8.

For reference, Fig. 7 shows the power threshold quantified by the right side of (15) for this sensor configuration (sensors again shown as diamonds), as a grayscale map in the region  $\Omega$ , with the sensors positions shown as diamonds.

**E. AN ALGORITHMIC IMPROVEMENT**

The clearance criterion (15) can be used to improve the results of reconstructions. Specifically, we:

- 1) Run the BLOOMP algorithm with a given termination tolerance of the form (6). Let  $\epsilon$  denote the tolerance used on  $\|\mathbf{d} - \mathbf{d}_k\|_2$  to terminate the iterations in BLOOMP, e.g.,  $\epsilon = C\sqrt{(\mu_0^2 + \sigma_0^2)}\|\mathbf{d}\|_2$  for some  $C$ .
- 2) Apply the clearance criteria (15) to each potential emitter location, using the 2-norm for  $\|\Phi_i\|$ , eliminating any recovered emitter that does not exceed the threshold.

The effect of Step 2 above is to “clean up” reconstructions, by eliminating estimated emitters that are more likely the result of noise. This threshold can be applied more or less

aggressively in the form

$$P > C' \frac{2\epsilon}{\|\Phi_i\|} \tag{16}$$

by choosing  $C'$  to be something other than 1. A larger value of  $C'$  more aggressively eliminates spurious emitter estimates.

To illustrate, we reconsider the reconstruction of Fig. 1, using the termination criterion (6) with  $C = 0.25$  (the same as was used in Fig. 1.) In Fig. 8 we show the recovery obtained without using the clearance criteria; this figure would be identical to Fig. 1, but here we display only the “low power” emitter recoveries, those with power less than 0.5. Moreover, all such emitters are shown at the same gray-level.

Low Power Emitter Estimates, No Clearance Threshold

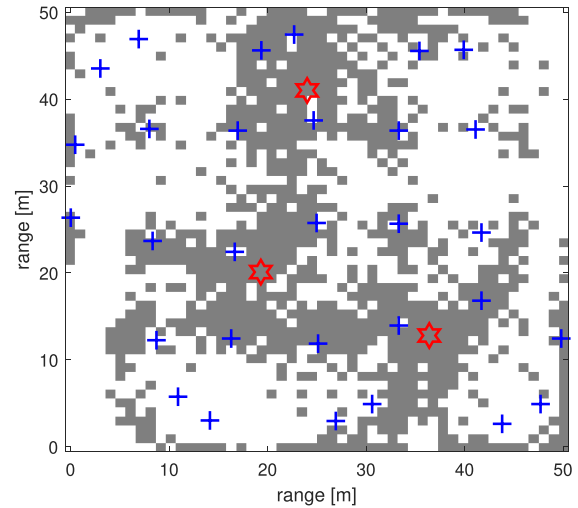


FIGURE 8. Setting of Fig. 1, no clearance threshold used, recovered emitters of power less than 0.5 only shown.

If we apply the clearance criteria (16) with  $C' = 1$  (applied to each of the 500 reconstructions individually) we obtain the analogous result of Fig. 9. As one might expect based on Fig. 7, the areas far from any sensor have higher power thresholds; emitters recovered in these areas must be stronger to exceed the threshold, since they are more likely spurious, many of the erroneously estimated emitters of small power in Fig. 8 have been removed in Fig. 9.

Figs. 10 and 11 illustrate the same situation but in which the log-normal noise is at 5 dB (in this case the signal-to-noise ratio is about 3.4, or  $-10.6$  dB.) As in the previous setting, the clearance criteria (16) is applied with  $C' = 1$ , to each of the 500 reconstructions individually.

**V. ILLUSTRATION WITH MEASURED DATA**

In this section we briefly detail an experiment that we, with the aid of our students, performed to collect actual RSS data under conditions that were only simulated above. Our goal here is not to reproduce the resolution or clearance analysis with experimentation, but rather to estimate realistic noise and pathloss parameters under relatively ideal conditions, and then perform a reconstruction for a single emitter, to illustrate

Low Power Emitters, Clearance Threshold Applied

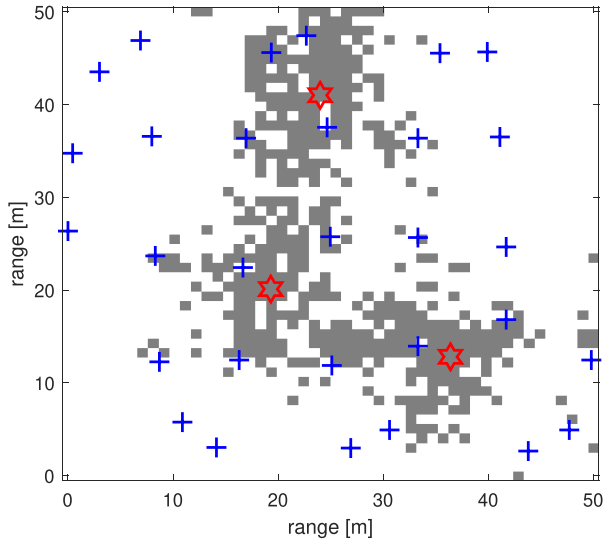


**FIGURE 9.** Setting of Fig. 1, clearance threshold used, recovered emitters of power less than 0.5 only shown.

Low Power Emitters, Clearance Threshold Applied

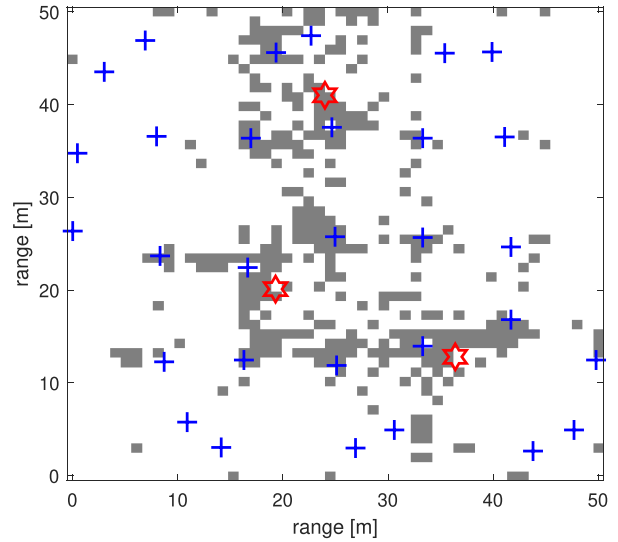


**FIGURE 11.** Setting of Fig. 1 with 5 dB log-normal noise, clearance threshold used, recovered emitters of power less than 0.5 only shown.

Low Power Emitter Estimates, No Clearance Threshold

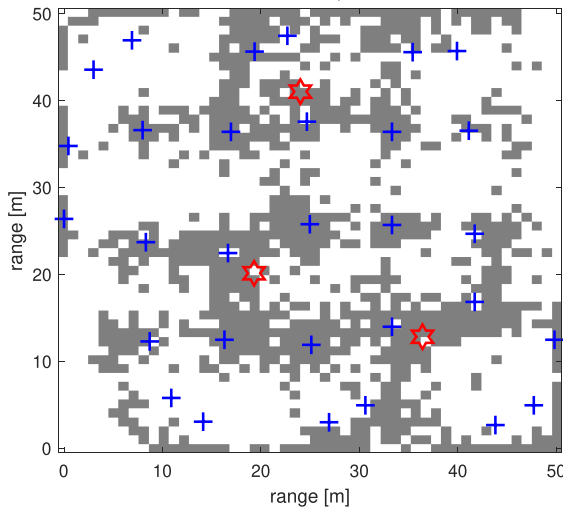


**FIGURE 10.** Setting of Fig. 1 with 5 dB log-normal noise, no clearance threshold used, recovered emitters of power less than 0.5 only shown.

the effectiveness of the proposed algorithms and modification via (16).

**A. MEASUREMENT OF RSS IN OPEN AIR**

An experiment to collect RSS data from a single emitter using 13 sensors was conducted in the open-air on a flat grass-covered field of 90 × 120 meters with no overhead obstructions. The transmitter was placed at location (12.4, 17.5) meters relative to an origin on a cartesian grid, at a height of 70 cm. Thirteen different receivers were scattered within a 50 × 50 meter square area to collect RSS samples at 13 different positions  $s_j$ . The height of the receivers was 50 cm. The  $xy$  locations of the receivers and emitter are plotted in Fig. 13. This is similar to the configurations we simulated in Sections IV, though with the emitter and sensors at approximately the same height.

The emitter transmitted a continuous-wave, unmodulated signal, centered at 925 MHz (in the ISM band) using a Software Defined Radio (SDR) transceiver (USR P E100, Ettus Research). An omnidirectional vertical dipole antenna was used for the transmitter (VERT900, Ettus Research). The transmitted signal was sampled at each sensor position at a rate of 1.152 Msamples/s, for a duration of one second, using an SDR radio (receiver only) device with a USB interface (R820T NESDR Mini, Noo Electric). The RTL-SDR has the capability to tune over the range 25 MHz to 1.75 GHz, producing raw, 8-bit IQ data samples, at a programable, base-band sampling rate of up to 2.8MHz [43]. However, the data acquisition sampling rate was set lower to ensure the accuracy of the rate. The gain was set to 32.8 for each of the receivers, which was tuned so that the receiver closest to the transmitter ( $\approx 6.5$  meters away) did not experience saturation. Without automatic gain control, we found the useful dynamic range of the RTL-SDR is around 45 dB. The receivers used an omnidirectional vertical dipole antenna, approximately 14 cm in length with an MCX connection.

The raw IQ data were processed using the procedures recommended in [35]. The RSS was calculated by first applying a Chebyshev Type I IIR filter of order 1 to remove most of the fast-fading variations. A least-squares fit to the log-normal distance trend is used to estimate the path-length exponent,  $n \approx 3.45$  for our data. The standard deviation of the log-normalized uncertainty term (long-term fading uncertainty) was computed from the variation from the fitted data,  $\sigma_{dB} = 1.86$  dB. The decimated RSS values and fit are plotted in Fig. 12.

**B. A SAMPLE RECONSTRUCTION FROM DATA**

In the reconstructions that follow the RSS values were normalized to correspond to an emitter power (non-dimensional) of 1 at a distance of 1 meter, as in the simulations above.

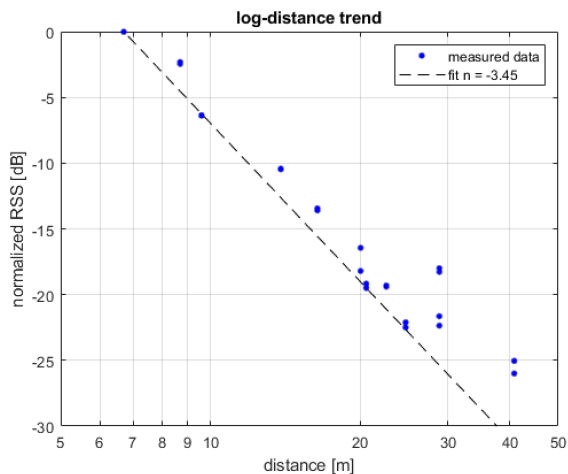


**FIGURE 12.** The normalized RSS measured from sensors randomly placed in a 50 × 50 meter search area are plotted (dots). Measurements were repeated to obtain a better estimate of the channel propagation variance. The log-linear fit is displayed as the dashed line. The pathloss trend predicted by the free-space approximation is displayed as a solid black line.

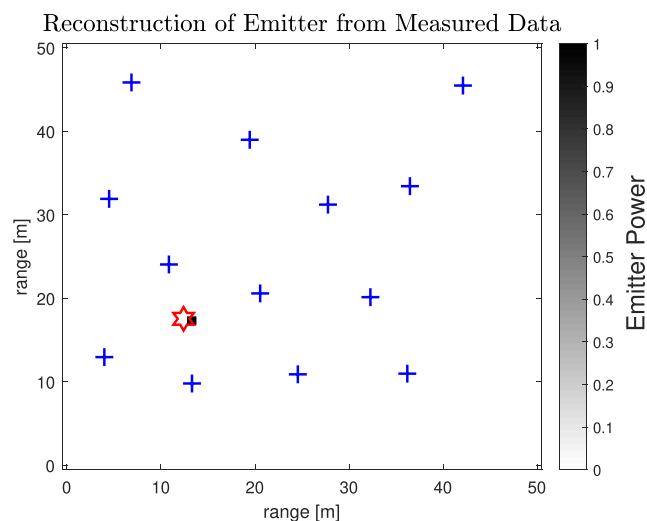


**FIGURE 13.** The emitter was placed at the position (12.41 m, 17.56 m) as indicated by the red asterisk. The sensor locations are marked by blue crosses. An estimate of the emitter’s location as computed by the BLOOMP algorithm is at the position (12.50 m, 15.50 m), indicated by a black square.

To begin, we show a reconstruction of the emitter location using the BLOOMP algorithm with data from all 13 sensors. Band exclusion is applied to the modified BLOOMP algorithm according to [39] with a exclusion parameter set to 0.95. We use the pathloss exponent  $n = 3.45$  estimated above and assume noise level  $\sigma_{dB} = 2$  dB. The BLOOMP termination criteria is as given in (6) with  $C = 0.25$ . The algorithm in fact terminates in one iteration (and as a result, estimates that only one emitter is present). In Fig. 13, the estimated location of the emitter is plotted as the single black square, with the true emitter indicated by the red asterisk. The estimate falls on the closest grid point at (12.50 m, 15.50 m) which is 1.1 meters

away from the position of the true emitter’s location (12.41 m, 17.56 m). It should be noted that the true emitter itself is not on a grid point. The recovered power estimate was 1.15.

**C. CLEARANCE THRESHOLD APPLIED TO DATA**

In this section we illustrate the reconstruction of the emitter location using relatively few sensors, and how the clearance criterion can be used to “clean up” reconstructions and eliminate (likely) spurious emitter estimates.

An often cited rule-of-thumb regarding compressed sensing estimates for sparse solutions is that the number of data points should be at least four times the sparsity of the unknown solution [41]. However, this rule applies to situations in which the measurement matrix has relatively low coherence—not the present case. As such, we expect that the reliable recovery of even a single emitter from RSS data should require somewhat more than 4 sensors. In the examples that follow we used subsets of 7 sensors, chosen from the 13 we have available, so approximately half of the sensors are involved in any given reconstruction.

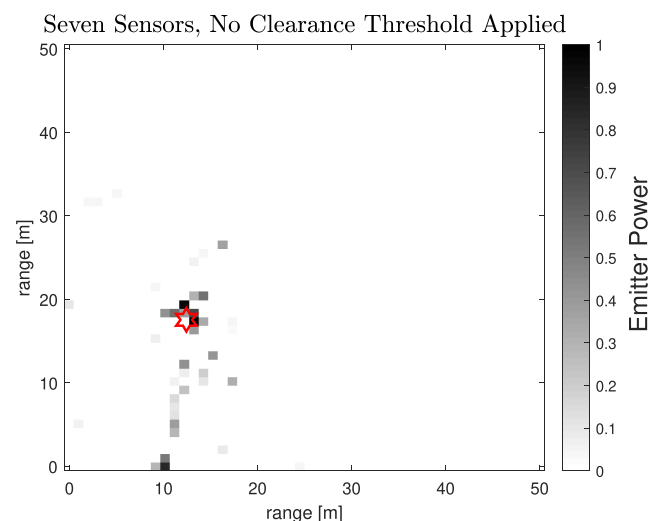


**FIGURE 14.** Average of 146 reconstructions using 7 emitters in each case, with emitter power rescaled logarithmically. No clearance power threshold applied.

In Fig. 14 is shown the average of 146 reconstructions using the 146 subsets of our 13 sensors that satisfy the criteria of being “spatially diverse.” Specifically, we require that no two sensors are closer than 10 meters, and at least two are separated by 50 meters or more, in order to provide adequate coverage of the 50 × 50 meter field. For each reconstruction we iterate the BLOOMP algorithm with a rather stringent termination criterion, (6) with  $C = 0.1$ . This has the effect of causing the algorithm to overfit the data and gives rise to spurious small emitters. We then plot the recovered emitter powers with the rescaling  $p \rightarrow \log(1 + 100p)/\log(101)$ , in order show the low power emitter estimates that are recovered. We do not apply the clearance threshold (15) in this reconstruction.

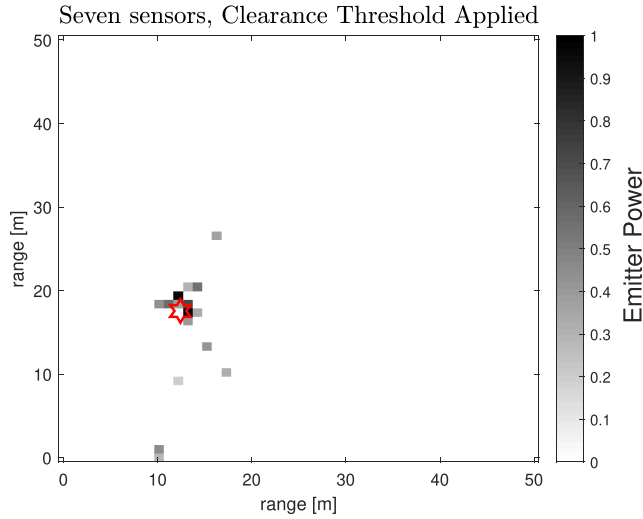


**FIGURE 15. Average of 146 reconstructions using 7 emitters in each case, with emitter power rescaled logarithmically and clearance power threshold applied.**

In Fig. 14 we see numerous spurious emitter estimates. In fact, the algorithm recovers an average of 1.62 emitters per reconstruction, generally one emitter of power approximately 1, others with much smaller power. In Fig. 15 we show the result of applying the clearance criterion (16) with  $C' = 1$  to each reconstruction individually. The application of the clearance criterion effectively eliminates many spurious emitter estimates, in a way that incorporates the position of the emitters relative to the sensor geometry and the noise level in the data. This also has the benefit of taking some of the premium off of choosing precisely the correct tolerance on the right in the termination criterion (6), since spurious estimates are eliminated. In fact, the average sparsity of the data after application of the clearance criterion is exactly 1.0 (though clearly not all reconstructions are perfect).

**VI. CONCLUSION**

We have considered the problem of using a limited number of low-capability sensors to geolocate an unknown number of RF emitters with indistinguishable transmission characteristics in a given region. We have formulated this as a problem in compressed sensing. We then used this formulation to quantify the limits on resolution and emitter detectability as a function of the data noise level, sensor number and placement, as well as other relevant variables, for example, the pathloss exponent. This analysis also allows us to implement an effective algorithm for recovering multiple emitters, both their location and power, from relatively few sensors, in the presence of realistic noise. We have demonstrated the effectiveness of this algorithm on both synthetic and real data.

Several natural extensions and refinements of this technique suggest themselves. The model can be easily adapted to directional sensor antennas, and emitters (or sensors) at nonuniform altitude. Also of interest, but more challenging, is the problem of locating anisotropic, intermittent, or moving emitters, and operating in an environment in which sensor

positions themselves are not known and must be estimated. We also intend, in future work, to validate this approach using real data collected from multiple emitters.

**APPENDIX A**

As noted in Section III-B, we iterate the BLOOMP algorithm until the fit squared residual is comparable to  $E(\|\mathbf{d} - \mathbf{d}_0\|_2^2)$ . The latter quantity can be estimated from  $\mathbf{d}$  (the measured data) and the noise level  $\sigma_{dB}$ .

From the noise-free model (1) and noisy model (3) we compute

$$\|\mathbf{d} - \mathbf{d}_0\|_2^2 = d_0^{2n} \sum_{i=1}^M \left( \sum_{j=1}^N \frac{p_j}{r_{i,j}^n} X_{i,j} \right)^2 \tag{17}$$

where  $X_{i,j} = e^{\eta R_{i,j}/10} - 1$  with  $R_{i,j}$  normal with mean zero, variance  $\sigma_{dB}^2$ . The random variable  $X_{i,j}$  is log-normal with mean and variance given by

$$\mu_0 = e^{\eta^2 \sigma_{dB}^2 / 2} - 1, \quad \sigma_0^2 = e^{\eta^2 \sigma_{dB}^2} (e^{\eta^2 \sigma_{dB}^2} - 1). \tag{18}$$

Since the expected value is linear we have

$$E(\|\mathbf{d} - \mathbf{d}_0\|_2^2) = d_0^{2n} \sum_{i=1}^M E \left[ \left( \sum_{j=1}^N \frac{p_j}{r_{i,j}^n} X_{i,j} \right)^2 \right]. \tag{19}$$

A little algebra shows that

$$\begin{aligned} E \left[ \left( \sum_{j=1}^N \frac{p_j}{r_{i,j}^n} X_{i,j} \right)^2 \right] &= E \left[ \sum_{j,k=1}^N \frac{p_j p_k}{r_{i,j}^n r_{i,k}^n} X_{i,j} X_{i,k} \right] \\ &= \sum_{j,k=1}^N \frac{p_j p_k}{r_{i,j}^n r_{i,k}^n} E(X_{i,j} X_{i,k}) \\ &= \sum_{j=1}^N \frac{p_j^2}{r_{i,j}^{2n}} E(X_{i,j}^2) \\ &\quad + \sum_{j,k=1, j \neq k}^N \frac{p_j p_k}{r_{i,j}^n r_{i,k}^n} E(X_{i,j} X_{i,k}). \end{aligned} \tag{20}$$

Since the  $X_{i,j}$  are independent we have

$$\begin{aligned} E(X_{i,j} X_{i,k}) &= E(X_{i,j}) E(X_{i,k}) = \mu_0^2 \\ E(X_{i,j}^2) &= \mu_0^2 + \sigma_0^2. \end{aligned}$$

Then some mundane algebra shows that

$$\begin{aligned} E(\|\mathbf{d} - \mathbf{d}_0\|_2^2) &= d_0^{2n} \sum_{i=1}^M \left( (\mu_0^2 + \sigma_0^2) \sum_{j=1}^N \frac{p_j^2}{r_{i,j}^{2n}} \right. \\ &\quad \left. + \mu_0^2 \sum_{j,k=1, j \neq k}^N \frac{p_j p_k}{r_{i,j}^n r_{i,k}^n} \right) \\ &= d_0^{2n} \sum_{i=1}^M \left( \mu_0^2 \sum_{j,k=1}^N \frac{p_j p_k}{r_{i,j}^n r_{i,k}^n} + \sigma_0^2 \sum_{j=1}^N \frac{p_j^2}{r_{i,j}^{2n}} \right) \end{aligned}$$



$$\begin{aligned}
&= d_0^{2n} \sum_{i=1}^M \left( \mu_0^2 \left( \sum_{j=1}^N \frac{P_j}{r_{i,j}^n} \right)^2 + \sigma_0^2 \sum_{j=1}^N \frac{P_j^2}{r_{i,j}^{2n}} \right) \\
&= \mu_0^2 \|\mathbf{d}_0\|_2^2 + \sigma_0^2 d_0^{2n} \sum_{i=1}^M \sum_{j=1}^N \frac{P_j^2}{r_{i,j}^{2n}} \\
&\leq \mu_0^2 \|\mathbf{d}_0\|_2^2 + \sigma_0^2 d_0^{2n} \sum_{i=1}^M \sum_{j,k=1}^N \frac{P_j P_k}{r_{i,j}^n r_{i,k}^n} \\
&= \mu_0^2 \|\mathbf{d}_0\|_2^2 + \sigma_0^2 \sum_{i=1}^M \left( d_0^n \sum_j \frac{P_j}{r_{i,j}^n} \right)^2 \\
&= \mu_0^2 \|\mathbf{d}_0\|_2^2 + \sigma_0^2 \|\mathbf{d}_0\|_2^2 \\
&= (\mu_0^2 + \sigma_0^2) \|\mathbf{d}_0\|_2^2. \tag{21}
\end{aligned}$$

This provides the basis for the termination criterion (6) (replacing  $\mathbf{d}_0$  with  $\mathbf{d}$ ).

Note however that  $E(\|\mathbf{d} - \mathbf{d}_0\|_2^2) \geq E(\|\mathbf{d} - \mathbf{d}_0\|_2)^2$ , so the termination criterion (6) may result in under-fitting the data. When  $\sigma_{dB} \leq 5$  the quantities  $E(\|\mathbf{d} - \mathbf{d}_0\|_2^2)$  and  $E(\|\mathbf{d} - \mathbf{d}_0\|_2)^2$  are comparable in magnitude, but for larger noise levels the random variable  $\|\mathbf{d} - \mathbf{d}_0\|_2$  is skewed heavily higher, to the right. In such a case a smaller value of  $C$  in (6) is appropriate.

## ACKNOWLEDGMENTS

The authors would like to thank the many Rose-Hulman undergraduate and master's students who have worked with us on this project (and continue to do so). Dr. Walter would also like to thank the many colleagues at the Air Force Research Laboratory Sensors Directorate who have supported her.

## REFERENCES

- [1] A. H. Sayed, A. Tarighat, and N. Khajehnouri, "Network-based wireless location: Challenges faced in developing techniques for accurate wireless location information," *IEEE Signal Process. Mag.*, vol. 22, no. 4, pp. 24–40, Jul. 2005, doi: [10.1109/MSP.2005.1458275](https://doi.org/10.1109/MSP.2005.1458275).
- [2] H. Jamali-Rad, "Sparsity-aware wireless networks: Localization and sensor selection," Ph.D. dissertation, Dept. Microelectron. Comput. Eng., TU Delft, Delft, The Netherlands, 2014.
- [3] C. Feng, W. S. A. Au, S. Valaee, and Z. Tan, "Received-signal-strength-based indoor positioning using compressive sensing," *IEEE Trans. Mobile Comput.*, vol. 11, no. 12, pp. 1983–1993, Dec. 2012, doi: [10.1109/TMC.2011.216](https://doi.org/10.1109/TMC.2011.216).
- [4] A. J. Weiss, "On the accuracy of a cellular location system based on RSS measurements," *IEEE Trans. Veh. Technol.*, vol. 52, no. 6, pp. 1508–1518, Nov. 2003, doi: [10.1109/TVT.2003.819613](https://doi.org/10.1109/TVT.2003.819613).
- [5] N. Patwari, J. N. Ash, S. Kyperountas, A. O. Hero, R. L. Moses, and N. S. Correal, "Locating the nodes: Cooperative localization in wireless sensor networks," *IEEE Signal Process. Mag.*, vol. 22, no. 4, pp. 54–69, Jul. 2005, doi: [10.1109/MSP.2005.1458287](https://doi.org/10.1109/MSP.2005.1458287).
- [6] P. Daponte, L. De Vito, F. Picariello, S. Rapuano, and I. Tudosa, "Compressed sensing technologies and challenges for aerospace and defense RF source localization," in *Proc. 5th IEEE Int. Workshop Metro. AeroSpace (MetroAeroSpace)*, Rome, Italy, Jun. 2018, pp. 634–639, doi: [10.1109/MetroAeroSpace.2018.8453560](https://doi.org/10.1109/MetroAeroSpace.2018.8453560).
- [7] J. A. Bazerque and G. B. Giannakis, "Distributed spectrum sensing for cognitive radio networks by exploiting sparsity," *IEEE Trans. Signal Process.*, vol. 58, no. 3, pp. 1847–1862, Mar. 2010, doi: [10.1109/TSP.2009.2038417](https://doi.org/10.1109/TSP.2009.2038417).
- [8] X. Li, Q. Han, V. Chakravarthy, and Z. Wu, "Joint spectrum sensing and primary user localization for cognitive radio via compressed sensing," in *Proc. Mil. Commun. Conf. (MILCOM)*, San Jose, CA, USA, Oct. 2010, pp. 329–334, doi: [10.1109/MILCOM.2010.5680334](https://doi.org/10.1109/MILCOM.2010.5680334).
- [9] M. S. Butler, "Low cost, low complexity sensor design for non-cooperative geolocation via received signal strength," M.S. thesis, Dept. Elect. Comput. Eng., Air Force Inst. Technol., Wright-Patterson AFB, OH, USA, 2012.
- [10] S. A. King, "Development of a model and localization algorithm for received signal strength-based geolocation," Ph.D. dissertation, Dept. Elect. Comput. Eng., Air Force Inst. Technol., Wright-Patterson AFB, OH, USA, 2013.
- [11] D. Walter, J. Klein, J. Kaupert, C. Bullmaster, and V. Chakravarthy, "Multiple UAV tomography based geolocation of RF emitters," *Proc. SPIE*, vol. 7707, Apr. 2010, Art. no. 77070B, doi: [10.1117/12.850168](https://doi.org/10.1117/12.850168).
- [12] D. J. Walter, K. Bryan, J. Stephens, C. Bullmaster, and V. Chakravarthy, "Localization of RF emitters using compressed sensing with multiple cooperative sensors," in *Proc. IEEE Nat. Aerosp. Electron. Conf. (NAECON)*, Dayton, OH, USA, Jul. 2012, pp. 236–240, doi: [10.1109/NAECON.2012.6531060](https://doi.org/10.1109/NAECON.2012.6531060).
- [13] Telefonaktiebolaget LM Ericsson. Accessed: Nov. 21, 2019. [Online]. Available: <https://www.ericsson.com/en/white-papers/drones-and-networks-ensuring-safe-and-secure-operations>
- [14] H. Rydén, S. B. Redhwan, and X. Lin, "Rogue drone detection: A machine learning approach," 2018, *arXiv:1805.05138*. Accessed: Nov. 21, 2019. [Online]. Available: <http://arxiv.org/abs/1805.05138>
- [15] P. Nguyen, M. Ravindranatha, A. Nguyen, R. Han, and T. Vu, "Investigating cost-effective RF-based detection of drones," in *Proc. 2nd Workshop Micro Aerial Vehicle Netw., Syst., Appl. Civilian Use (DroNet)*, Singapore, Jun. 2016, pp. 17–22.
- [16] I. Guvenc, F. Koohifar, S. Singh, M. L. Sicitu, and D. Matolak, "Detection, tracking, and interdiction for amateur drones," *IEEE Commun. Mag.*, vol. 56, no. 4, pp. 75–81, Apr. 2018, doi: [10.1109/MCOM.2018.1700455](https://doi.org/10.1109/MCOM.2018.1700455).
- [17] J. T. Adams, "An introduction to IEEE STD 802.15.4," in *Proc. IEEE Aerosp. Conf., Big Sky, MT, USA, Mar. 2006*, pp. 1–8, doi: [10.1109/AERO.2006.1655947](https://doi.org/10.1109/AERO.2006.1655947).
- [18] K. Whitehouse, C. Karlof, and D. Culler, "A practical evaluation of radio signal strength for ranging-based localization," *ACM SIGMOBILE Mobile Comput. Commun. Rev.*, vol. 11, no. 1, pp. 41–52, Jan. 2007, doi: [10.1145/1234822.1234829](https://doi.org/10.1145/1234822.1234829).
- [19] B. Fidan, S. Dasgupta, and B. D. O. Anderson, "Guaranteeing practical convergence in algorithms for sensor and source localization," *IEEE Trans. Signal Process.*, vol. 56, no. 9, pp. 4458–4469, Sep. 2008, doi: [10.1109/TSP.2008.924138](https://doi.org/10.1109/TSP.2008.924138).
- [20] E. P. de Freitas, T. Heimfarth, A. M. Ferreira, C. E. Pereira, F. R. Wagner, and T. Larsson, "Decentralized task distribution among cooperative UAVs in surveillance systems applications," in *Proc. 7th Int. Conf. Wireless On-Demand Netw. Syst. Services (WONS)*, Feb. 2010, pp. 121–128, doi: [10.1109/WONS.2010.5437123](https://doi.org/10.1109/WONS.2010.5437123).
- [21] V. Cevher, M. F. Duarte, and R. G. Baraniuk, "Distributed target localization via spatial sparsity," in *Proc. 16th Eur. Signal Process. Conf. (EUSIPCO)*, Lausanne, Switzerland, Aug. 2008, pp. 1–5.
- [22] C. Feng, S. Valaee, and Z. Tan, "Multiple target localization using compressive sensing," in *Proc. IEEE Global Telecommun. Conf. (GLOBECOM)*, Honolulu, HI, USA, Nov. 2009, pp. 1–6, doi: [10.1109/GLOBECOM.2009.5425808](https://doi.org/10.1109/GLOBECOM.2009.5425808).
- [23] A. C. Fannjiang, T. Strohmer, and P. Yan, "Compressed remote sensing of sparse objects," *SIAM J. Imag. Sci.*, vol. 3, no. 3, pp. 595–618, Jan. 2010, doi: [10.1137/090757034](https://doi.org/10.1137/090757034).
- [24] S. Whiting, "Radio-frequency transmitter geolocation using non-ideal received signal strength indicators," M.S. thesis, Dept. Elect. Comput. Eng., Univ. Utah, Salt Lake City, UT, USA, 2018.
- [25] P. Zuo, T. Peng, K. You, W. Guo, and W. Wang, "RSS-based localization of multiple directional sources with unknown transmit powers and orientations," *IEEE Access*, vol. 7, pp. 88756–88767, 2019.
- [26] T. Peng, P. Zuo, K. You, H. Jing, W. Guo, and W. Wang, "Bounds and methods for multiple directional sources localization based on RSS measurements," *IEEE Access*, vol. 7, pp. 131395–131406, 2019.
- [27] X. Tian, R. Shen, D. Liu, Y. Wen, and X. Wang, "Performance analysis of RSS fingerprinting based indoor localization," *IEEE Trans. Mobile Comput.*, vol. 16, no. 10, pp. 2847–2861, Oct. 2017, doi: [10.1109/TMC.2016.2645221](https://doi.org/10.1109/TMC.2016.2645221).

- [28] N. Patwari, A. O. Hero, M. Perkins, N. S. Correal, and R. J. O’Dea, “Relative location estimation in wireless sensor networks,” *IEEE Trans. Signal Process.*, vol. 51, no. 8, pp. 2137–2148, Aug. 2003, doi: [10.1109/TSP.2003.814469](https://doi.org/10.1109/TSP.2003.814469).
- [29] H. Koorapaty, “Barankin bounds for position estimation using received signal strength measurements,” in *Proc. IEEE 59th Veh. Technol. Conf. (VTC-Spring)*, vol. 5, May 2004, pp. 2686–2690, doi: [10.1109/VETECS.2004.1391408](https://doi.org/10.1109/VETECS.2004.1391408).
- [30] S. D. Chitte, S. Dasgupta, and Z. Ding, “Distance estimation from received signal strength under log-normal shadowing: Bias and variance,” *IEEE Signal Process. Lett.*, vol. 16, no. 3, pp. 216–218, Mar. 2009, doi: [10.1109/LSP.2008.2012229](https://doi.org/10.1109/LSP.2008.2012229).
- [31] S. D. Chitte, “Source localization from received signal strength under lognormal shadowing,” M.S. thesis, Dept. Elect. Comput. Eng., Univ. Iowa, Iowa City, IA, USA, 2010, pp. vii, doi: [10.17077/etd.getg4038](https://doi.org/10.17077/etd.getg4038).
- [32] R. Roy and T. Kailath, “ESPRIT-estimation of signal parameters via rotational invariance techniques,” *IEEE Trans. Acoust., Speech, Signal Process.*, vol. 37, no. 7, pp. 984–995, Jul. 1989, doi: [10.1109/29.32276](https://doi.org/10.1109/29.32276).
- [33] R. Schmidt, “Multiple emitter location and signal parameter estimation,” *IEEE Trans. Antennas Propag.*, vol. AP-34, no. 3, pp. 276–280, Mar. 1986, doi: [10.1109/TAP.1986.1143830](https://doi.org/10.1109/TAP.1986.1143830).
- [34] R. K. Martin, A. S. King, J. R. Pennington, R. W. Thomas, R. Lenahan, and C. Lawyer, “Modeling and mitigating noise and nuisance parameters in received signal strength positioning,” *IEEE Trans. Signal Process.*, vol. 60, no. 10, pp. 5451–5463, Oct. 2012, doi: [10.1109/TSP.2012.2207118](https://doi.org/10.1109/TSP.2012.2207118).
- [35] A. Zanella, “Best practice in RSS measurements and ranging,” *IEEE Commun. Surveys Tuts.*, vol. 18, no. 4, pp. 2662–2686, 4th Quart., 2016, doi: [10.1109/COMST.2016.2553452](https://doi.org/10.1109/COMST.2016.2553452).
- [36] S. Foucart and H. Rauhut, *A Mathematical Introduction to Compressive Sensing*. New York, NY, USA: Springer, 2013.
- [37] D. L. Donoho, M. Elad, and V. N. Temlyakov, “Stable recovery of sparse overcomplete representations in the presence of noise,” *IEEE Trans. Inf. Theory*, vol. 52, no. 1, pp. 6–18, Jan. 2006, doi: [10.1109/TIT.2005.860430](https://doi.org/10.1109/TIT.2005.860430).
- [38] B. K. Natarajan, “Sparse approximate solutions to linear systems,” *SIAM J. Comput.*, vol. 24, no. 2, pp. 227–234, Apr. 1995, doi: [10.1137/S0097539792240406](https://doi.org/10.1137/S0097539792240406).
- [39] A. Fannjiang and W. Liao, “Coherence pattern-guided compressive sensing with unresoloved grids,” *SIAM J. Imag. Sci.*, vol. 5, no. 1, pp. 179–202, Jan. 2012, doi: [10.1137/110838509](https://doi.org/10.1137/110838509).
- [40] D. L. Donoho, Y. Tsaig, I. Drori, and J.-L. Starck, “Sparse solution of underdetermined systems of linear equations by stagewise orthogonal matching pursuit,” *IEEE Trans. Inf. Theory*, vol. 58, no. 2, pp. 1094–1121, Feb. 2012, doi: [10.1109/TIT.2011.2173241](https://doi.org/10.1109/TIT.2011.2173241).
- [41] E. J. Candés and M. B. Wakin, “An introduction to compressive sampling,” *IEEE Signal Process. Mag.*, vol. 25, no. 2, pp. 21–30, Mar. 2008, doi: [10.1109/MSP.2007.914731](https://doi.org/10.1109/MSP.2007.914731).
- [42] N. Mehta, J. Wu, A. Molisch, and J. Zhang, “Approximating a sum of random variables with a lognormal,” *IEEE Trans. Wireless Commun.*, vol. 6, no. 7, pp. 2690–2699, Jul. 2007, doi: [10.1109/TWC.2007.051000](https://doi.org/10.1109/TWC.2007.051000).
- [43] R. W. Stewart, L. Crockett, D. Atkinson, K. Barlee, D. Crawford, I. Chalmers, M. McLernon, and E. Sozer, “A low-cost desktop software defined radio design environment using MATLAB, simulink, and the RTL-SDR,” *IEEE Commun. Mag.*, vol. 53, no. 9, pp. 64–71, Sep. 2015, doi: [10.1109/MCOM.2015.7263347](https://doi.org/10.1109/MCOM.2015.7263347).



**KURT BRYAN** (Member, IEEE) received the bachelor’s degree in mathematics from the Reed College, in 1984, and the Ph.D. degree in mathematics from the University of Washington, in 1990. He held a three year postdoctoral position with the NASA Langley Research Center. He was with Blount Industries, Portland, and Crane Payment Innovations. He has also held visiting positions with the U.S. Air Force Academy and Rutgers University. His research interests include

inverse problems, numerical analysis, signal and image processing, and involving undergraduates in applied mathematics research.



**DEBORAH J. WALTER** (Member, IEEE) received the B.S. degree in electrical engineering from the University of Maryland, College Park, in 1990, and the M.S. and Ph.D. degrees in electrical engineering from the Pennsylvania State University, State College, PA, USA, in 1994 and 1999, respectively. Since August 2006, she has been with the Department of Electrical and Computer Engineering, Rose-Hulman Institute of Technology, Terre Haute, IN, USA. She was with the GE Global

Research Center, Computed Tomography Laboratory. She is currently an Associate Professor with the Rose-Hulman Institute of Technology. Her research interests include signal processing, cognitive radio, source localization, and educational pedagogy.

...